Theory and boundary element methods for nearfield acoustic holography

Thomas DeLillo[1] Tomasz Hrycak[1] Victor Isakov[1]

July 2, 2004

Keywords. ill-posed problems, inverse problems in acoustics, iterative regularization, conjugate gradient, parameter choice strategies, Helmholtz equation, HELS method.

Short title. Boundary element methods for NAH.

This research was supported by NSF ITR/ACS grant 0081270.

Abstract

We consider the problem of recovering surface vibrations from acoustic pressure measurements taken in the interior or the exterior of a region. We give two formulations of the problem. One is based on a representation of the pressure as layer potentials and the other is based on approximation by a class of specific solutions to the Helmholtz equation. Boundary element methods are developed to approximate the integral operators. A conjugate gradient algorithm based on Lanczos bidiagonalization is applied to compute regularized solutions to the ill-conditioned equations in the presence of measurement errors. Numerical examples which compare the two formulations are presented.

[1]Department of Mathematics and Statistics, Wichita State University, Wichta, KS 67260, email: delillo@math.twsu.redu, hrycak@math.twsu.edu, victor.isakov@wichita.edu

1 Introduction

Let Ω be a bounded domain in $\mathbf{R}^n$, $(n = 2, 3)$, with the Lipschitz boundary and connected complement $\Omega_+ = \mathbf{R}^n \setminus \bar{\Omega}$. We consider the acoustical pressure field u of frequency k satisfying the Helmholtz equation

$$\Delta u + k^2 u = 0 \quad \text{in} \quad \Omega \quad (\text{or in } \Omega_+ = \mathbf{R}^n \setminus \overline{\Omega}). \tag{1}$$

We are interested in applications where Ω is a cabin of an aircraft or an automobile. Solutions to (1) in Ω_+ are assumed to satisfy the Sommerfeld radiation condition

$$\lim r^{\frac{n-1}{2}} (\partial_r u - iku)(x) = 0, \qquad \text{as } r = |x| \to \infty \tag{2}$$

Such functions u are called radiating solutions. Pressure measurements are taken by acoustical sensors located on a surface Γ_0 inside or outside the cabin. Our goal is to reconstruct u inside Ω, or the normal velocity $v = \partial_\nu u$ on $\Gamma = \partial\Omega$, (ν is the unit exterior normal to $\partial\Omega$).

In Section 2, we show that uniqueness of the reconstruction depends on our choice of Γ_0. We also give stability estimates suggesting that in some cases stability increases with k. In Section 3, we describe a unique representation of u in Ω by the boundary layer potentials and discuss the potential representation for the exterior problem. This approach in principle allows us to handle numerically arbitrary domains Ω, while many existing methods are tailored to special domains Ω, where the Green's function of the Neumann problem for the Helmholtz equation can be found explicitly. Section 4 contains some approximation and completeness results. Section 5 describes our numerical methods and Section 6 discusses our regularization methods. Section 7 presents the results of three representative sets of computations comparing the methods.

In this paper, $H_{(m)}(\Omega)$ denotes the Sobolev space of functions on Ω whose partial derivatives up to order m are square integrable over Ω, and $\| \; \|_{(m)}$ denotes the standard norm on this space. We set $\| \; \|_2 = \| \; \|_{(0)}$ to be the norm in the space $L_2(\Omega)$.

2 Uniqueness and stability for the inverse problem

In this section we discuss uniqueness and stability of the continuation of solutions to (1). We denote by Ω_0 a Lipschitz domain with the closure $\bar{\Omega}_0$ contained in Ω for the interior problem or in Ω_+ for the exterior one.

Lemma 2.1 *Let k^2 be distinct from a Dirichlet eigenvalue of Ω_0. If $\Gamma_0 = \partial\Omega_0$, then $u \in H_{(1)}(\Omega)$ solving (1) is uniquely determined by its values on Γ_0.*

To prove uniqueness, we assume that $u = 0$ on Γ_0 and we have to conclude that $u = 0$ in Ω. Since k^2 is not a Dirichlet eigenvalue, a solution to the Dirichlet problem in Ω_0 is unique, so $u = 0$ in Ω_0. From uniqueness of the continuation from Ω_0 onto Ω (see [I], section 3.3), we conclude that $u = 0$ in Ω.

For the exterior problem uniqueness also holds when $\bar{\Omega} \subset \Omega_0$. Indeed, since a solution of the (exterior) Dirichlet problem with the data on $\partial\Omega_0$ is unique, then $u = 0$ on Γ_0 implies that $u = 0$ outside Ω_0 and hence, by uniqueness of the continuation, in Ω_+.

Nonuniqueness caused by the Dirichlet eigenvalues of Ω_0 cannot be avoided, but we can modify the eigenvalues by changing the measurement surface Γ_0. If k^2 is away from the Dirichlet eigenvalues, the Dirichlet problem in Ω_0 is stable in classical Sobolev (or Hölder) spaces. The problem of the continuation of solutions of elliptic equtions (from Ω_0 onto Ω) is notoriously unstable; however, assuming that $\|u\|_2(\Omega) < M_0$, one can control exponentially growing solutions and obtain the following conditional Hölder estimate

$$\|u\|_{(k)}(\Omega_1) \leq CM^{1-\lambda}\|u\|_2^{\lambda}(\Omega_0), \tag{3}$$

where C and λ $(0 < \lambda < 1)$ depend on Ω, Ω_0, k, and on the distance from $\Omega_1 \subset \Omega$ to $\partial\Omega$. We refer for proofs to [I], sections 3.2, 3.3. In the general situation, it is hard to get explicit bounds for either C or λ.

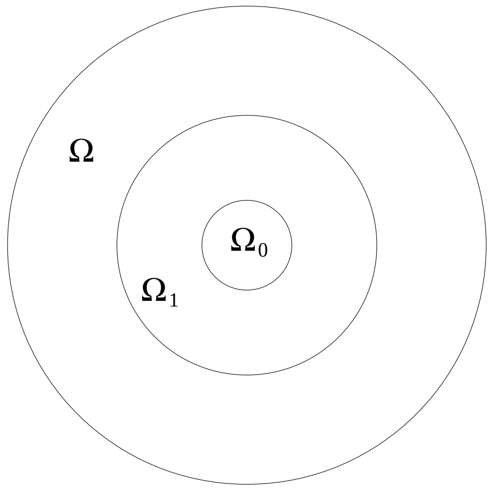

Figure 1: Geometry of the interior problem. In Theorem 2.1, $\Omega_0 = \Omega(r_0)$, $\Omega_1 = \Omega(r)$, and $\Omega = \Omega(r_1)$.

We now present a stability estimate for a special case when the domains in question are spheres in $\mathbf{R}^3$: $\Omega = \{|x| < r_1\}$ and $\Omega_0 = \{|x| < r_0\}$. For this geometry (see Figure 1), we derive almost explicit constants. It is well-known, that a solution u to the Helmholtz equation (1) in Ω admits the expansion $u(x) = \sum u_{m,n} j_n(kr) Y_{m,n}(\sigma)$, where j_n is the n-th spherical Bessel function, $r = |x|, \sigma = \frac{x}{r}$, and $Y_{m,n}$ are the spherical harmonics on the unit sphere. We denote by u_0 the sum of the terms with $n \leq n_1 = \frac{kr_1^2 - 3}{2}$, and by u_1 the sum of the remaining terms of the series. Let $\Omega(r) = \{|x| < r\}$.

Theorem 2.1 *Let u be a solution to the Helmholtz equation (1) in the ball $\Omega(r_1)$ and*

$$\|u\|_2(\Omega(r_1)) \leq M_0,\ \|\nabla u\|_2(\Omega(r_1)) \leq M_1. \tag{4}$$

Then

$$\frac{r_0^3}{r^2}\|u\|_2^2(\partial\Omega(r)) \leq C_1(r)\varepsilon_0^2 + C_2\varepsilon_1^{2\lambda}, \quad r < r_1 \tag{5}$$

where $\varepsilon_j^2 = \|u_j\|_2^2(\partial\Omega(r_0))$, $C_1(r) = max|\frac{j_n(kr)}{j_n(kr_0)}|^2$ *over* $n \leq n_1$, $C_2 = 5M^2$, $M^2 = 4M_0^2 + r_1^2 M_1^2$, *and* $\lambda = \frac{lnr_1 - lnr}{lnr_1 - lnr_0}$. *Moreover,*

$$\|u\|_2^2(\partial\Omega(r_1)) \leq C_1(r_1)\varepsilon_0^2 + C_3\varepsilon_2(C_4 - ln\varepsilon_2), \tag{6}$$

where $C_3 = \frac{1}{r_0}max(k^2M_0^2, M_1^2)ln\frac{r_1}{r_0}$, $\varepsilon_2 = -\frac{1}{ln\frac{\varepsilon_1}{M}}$, *and* $C_4 = 1 - ln\frac{r_0^3 C_3}{5M^2}$.

A proof of this stability estimate is given in [DIVW2]. It is based on explicit series representations and corresponding bounds for Bessel functions and on the logarithmic convexity method. We observe that C_1 can be easily calculated and it is relatively small. Since the number of terms included in u_1 grows, one expects an increased stability with increasing frequency. Indeed, this is observed in practical computations for nearfield acoustical holography [DIVW1], [DIVW2] for relatively small wave numbers k. However, according to classical results of Fritz John [J], stability of interior problems does not increase with frequency over the whole range of k. In fact, he constructed examples where stability deteriorates with increasing k. Recently, it has been rigorously proven that for the certain exterior problems stability indeed increases with k.

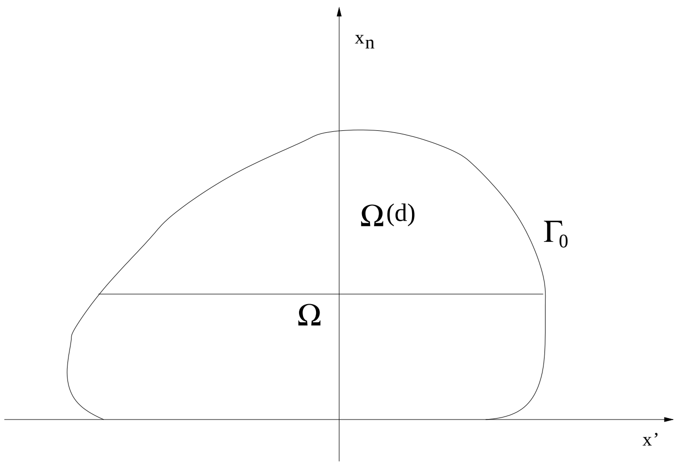

Figure 2: Geometry of continuation into the convex hull of Ω_0.

In the next theorem $\Omega \subset \{x_1^2 + ... + x_{n-1}^2 < r^2, 0 < x_n < h\}$, $\Omega(d) = \Omega \cap \{x_n > d\}$, and $\Gamma_0 = \partial\Omega \cap \{x_n > 0\}$, see Figure 2.

Theorem 2.2 *There is a constant C not depending on d, k such that*

$$\|u\|(\omega(d)) \leq C \left(\|u\|_2(\Gamma_0) + \|\nabla u\|_2(\Gamma_0) + \frac{\|u\|_{(1)}(\Omega)^{1-\lambda} \|u\|_{(1)}^{\lambda}(\Gamma_0)}{d(k+1)} \right) \tag{7}$$

for all solutions u to the Helmholtz equation (1). Here

$$\lambda = \frac{16r^2 d + 3d^2}{32r^2 h + h^2 d + 10d^2 h + 3d^2 + 24r^2 d}.$$

This bound and its implications are obtained in [HI] by using Carleman estimates for the Helmholtz equation with constants not depending on k. We observe that $0 < \lambda < 1$, and λ is decreases to 0 with d, i.e. when $\Omega(d)$ is approaching Ω.

3 Representation by potentials.

In the first approach we use the single and double layer potentials

$$\begin{aligned} S_\Gamma \varphi(x) &= \int_\Gamma \Phi(x,y)\varphi(y) d\Gamma(y), \\ D_\Gamma \varphi(x) &= \int_\Gamma \partial_{\nu(y)} \Phi(x,y)\varphi(y) d\Gamma(y), \quad x \in \Omega \text{ (or } x \in \Omega_+), \end{aligned} \tag{8}$$

where Φ is the free space radiating fundamental solution to (1) in $\mathbf{R}^n$. We recall that

$$\begin{aligned} \Phi(x,y) &= \frac{1}{4\pi} \frac{e^{ik|x-y|}}{|x-y|} \qquad \text{when } n = 3, \\ \Phi(x,y) &= \frac{i}{4} H_0^{(1)}(k|x-y|) \qquad \text{when } n = 2, \end{aligned} \tag{9}$$

where $H_0^{(1)}$ is the Hankel function. To formulate our results, it is convenient to fix a ball B containing $\overline{\Omega}$.

Theorem 3.1 *For any solution $u \in H_{(1)}(\Omega)$ to the Helmholtz equation (1), there is a unique function $\varphi \in H_{(-\frac{1}{2})}(\Gamma)$ such that $u(x) = S_\Gamma \varphi(x)$ for all $x \in \Omega$. Moreover, for some constant C depending only on Ω, we have*

$$C^{-1} \|u\|_{(1)}(\Omega) \leq \|\varphi\|_{(-\frac{1}{2})}(\Gamma) \leq C \|u\|_{(1)}(\Omega).$$

It is known that the trace operator $u \to u|_{\partial\Omega}$ maps $H_{(1)}(\Omega)$ into $H_{(\frac{1}{2})}(\partial\Omega)$. Additionally, the operator $u \to \partial_\nu u|_{\partial\Omega}$ is bounded from $H_{(1)}(\Omega)$ to $H_{(-\frac{1}{2})}(\partial\Omega)$. In both cases, the trace operators are first defined on smooth functions, and then extended by continuity.

We outline a proof of Theorem 3.1 referring for details to [DIVW2]. It is well-known, that the single layer potential S with density in $H_{(-\frac{1}{2})}(\Gamma)$ has the following properties:

$$-\Delta S_- - k^2 S_- = 0 \qquad \text{in } \Omega,\ -\Delta S_+ - k^2 S_+ = 0 \qquad \text{in } \Omega_+,$$
$$S_- - S_+ = 0,\ \partial_\nu S_- - \partial_\nu S_+ = \varphi \qquad \text{on } \Gamma, \tag{10}$$

and S_+ satisfies the radiation condition at infinity. Here S_- coincides with S on Ω and S_+ coincides with S outside Ω. Let $g \in H_{(\frac{1}{2})}(\Gamma)$ be the trace of the function u on Γ. It is well-known, that for exterior problems there is a unique radiating solution $u_+ \in H_{(1)}(B \setminus \Omega)$ to the Helmholtz equation in Ω_+ with the Dirichlet data g on Γ. In addition, the solutions u, u_+ of the interior and of the exterior Dirichlet problems in Ω with the Dirichlet data g, have their traces $\partial_\nu u$, $\partial_\nu u_+$ in the Sobolev space $H_{(-\frac{1}{2})}(\Gamma)$. Let $\varphi = \partial_\nu u - \partial_\nu u_+$ on Γ. We claim that Theorem 3.1 holds for this φ.

Indeed, the functions u and $S\varphi$ on Ω, and u_+ and $S_+\varphi$ on its complement, satisfy the same Helmholtz equations and the same transmission conditions at Γ (10), as well as the radiation condition at infinity. A solution of this transmission problem is unique. Hence $u = S\varphi$ in Ω.

A similar result holds for exterior problems, provided that k^2 is not a Dirichlet eigenvalue of Ω.

Theorem 3.2 *Let k^2 be distinct from a Dirichlet eigenvalue of Ω. For any radiating solution $u \in H_{(1)}(B \setminus \overline{\Omega})$ to the Helmholtz equation (1), there is a unique function φ in $H_{(-\frac{1}{2})}(\Gamma)$ such that $u(x) = S_\Gamma \varphi(x)$ for $x \in \Omega_+$. Moreover, for some constant C depending only on Ω, we have*

$$C^{-1}\|u\|_{(1)}(B \setminus \overline{\Omega}) \leq \|\varphi\|_{(-\frac{1}{2})}(\Gamma) \leq C\|u\|_{(1)}(B \setminus \overline{\Omega}).$$

The proof is similar to the proof of Theorem 3.1. We observe that if k^2 is a Dirichlet eigenvalue of Ω, then the representation of Theorem 3.2 is not unique. To demonstrate this, we recall Green's representations [CoKr]

$$\begin{aligned} u(x) &= -D_\Gamma u(x) + S_\Gamma \partial_\nu u(x), \qquad x \in \Omega, \\ u_+(x) &= D_\Gamma u_+(x) - S_\Gamma \partial_\nu u_+(x), \qquad x \in \Omega_+, \end{aligned} \tag{11}$$

valid for solutions $u \in H_{(1)}(\Omega)$ of the Helmholtz equation (1) in Ω, and for radiating solutions $u_+ \in H_{(1)}(B \setminus \bar{\Omega})$ in Ω_+. Let u_0 be a solution of (1) with $u_0 = 0$ on $\partial\Omega$. By Green's formula,

$$0 = \int_\Gamma \partial_\nu u_0(y) \Phi(x,y) d\Gamma(y),\ x \in \Omega_+.$$

Therefore the nonzero density $\varphi = \partial_\nu u_0$ produces the zero exterior single layer potential. Due to Theorems 3.1, 3.2, our problem reduces to solving the linear integral equation

$$\int_\Gamma \Phi(x,y)\varphi(y) d\Gamma(y) = u(x), \quad x \in \Gamma_0. \tag{12}$$

After determining φ in the interior problem, one can find the normal velocity from the formula

$$v(x) = \frac{1}{2}\varphi(x) + \int_\Gamma \nabla_x \Phi(x,y) \cdot \nu(x)\varphi(y) d\Gamma(y), \quad x \in \Gamma, \tag{13}$$

which follows from Theorem 3.1 and the jump relations. For the exterior problem, the normal velocity is given by a similar formula with $\frac{1}{2}\varphi(x)$ replaced by $-\frac{1}{2}\varphi(x)$. Again, we assume that k^2 is not a Dirichlet eigenvalue.

Finally, we discuss a ubiquitous representation by the sum of single and double layer potentials (8). We recall the known jump relations for double layer potentials

$$\begin{aligned} D_{+\Gamma}\varphi(z) &= \frac{1}{2}\varphi(z) + D_\Gamma\varphi(z), \\ D_{-\Gamma}\varphi(z) &= -\frac{1}{2}\varphi(z) + D_\Gamma\varphi(z), \end{aligned} \tag{14}$$

where $+$ denotes the limit from the outside of Ω and $-$ denotes the limit from the inside of Ω.

Lemma 3.1 *If $u \in H_{(1)}(\Omega)$ is a solution to (1), then there exist unique functions $\varphi_j \in H_{(\frac{1}{2}-j)}(\Gamma), (j = 0, 1)$, such that*

$$u(x) = S_\Gamma\varphi_1(x) - D_\Gamma\varphi_0(x), \ x \in \Omega,$$

$$\frac{1}{2}\varphi_0(z) = S_\Gamma\varphi_1(z) - D_\Gamma\varphi_0(z), \ z \in \Gamma.$$

To show existence of φ_0 and φ_1, let $\varphi_0 = u, \varphi_1 = \partial_\nu u$ on Γ and let us use equation (11) for Ω. To obtain the second relation we let in the first equation $x \to z$ and use the jump relations (14) to pass to the limit. We discover that

$$u(z) = S_\Gamma\varphi_1(z) + \frac{1}{2}\varphi_0(z) - D_\Gamma\varphi_0(z), \tag{15}$$

and since $\varphi_0 = u$ on Γ, we obtain the second equation of Lemma 3.1.

To show uniqueness of φ_j, it suffices to let $u = 0$ and to deduce that $\varphi_j = 0$. Letting $x \to z$ in the first equation of Lemma 3.1 with $u = 0$ and using the jump relations (14), we obtain (15) with $u = 0$. Now from the second equation of Lemma 3.1 it follows that $\varphi_0 = 0$. Finally, from the first equation of Lemma 3.1, we have $S_\Gamma\varphi_1 = 0$ on Ω. Now Theorem 2.1 implies that $\varphi_1 = 0$.

Lemma 3.2 *Let $u \in H_{(1)}(B \setminus \Omega)$ (for any B) be a solution to (1) in Ω_+. There exist functions $\varphi_j \in H_{(\frac{1}{2}-j)}(\Gamma), (j = 0, 1)$, such that*

$$u(x) = -S_\Gamma\varphi_1(x) + D_\Gamma\varphi_0(x), \ x \in \Omega_+,$$

$$\frac{1}{2}\varphi_0(z) = -S_\Gamma\varphi_1(z) + D_\Gamma\varphi_0(z), \ z \in \Gamma.$$

The function φ_0 is unique. If k^2 is not a Dirichlet eigenvalue of Ω, then φ_1 is unique.

A proof is similar to the proof of Lemma 3.1.

Now we can write the Helmholtz-Kirchhoff system of integral equations for the interior inverse problem

$$u(x) = S_\Gamma \varphi_1(x) - D_\Gamma \varphi_0(x),\ x \in \Gamma_0 \subset \Omega, \tag{16}$$

$$\frac{1}{2}\varphi_0(z) = S_\Gamma \varphi_1(z) - D_\Gamma \varphi_0(z),\ z \in \Gamma, \tag{17}$$

and for the exterior problem

$$u(x) = -S_\Gamma \varphi_1(x) + D_\Gamma \varphi_0(x),\ x \in \Gamma_0 \subset \Omega_+, \tag{18}$$

$$\frac{1}{2}\varphi_0(z) = -S_\Gamma \varphi_1(z) + D_\Gamma \varphi_0(z),\ z \in \Gamma. \tag{19}$$

Finally, we discuss uniqueness for integral equations (12), (16)-(19).

Lemma 3.3 *(Interior problem)*
If k^2 is not a Dirichlet eigenvalue of Ω_0, then under the conditions of Lemma 3.1, a solution $\varphi \in H_{(-\frac{1}{2})}(\Gamma)$ to the equation (12) is unique, and a solution $(\varphi_0, \varphi_1) \in H_{(\frac{1}{2})}(\Gamma) \times H_{(-\frac{1}{2})}(\Gamma)$ to the Helmholtz-Kirchhoff system (16), (17) is unique.

This follows directly from Theorem 3.1, Lemma 2.1 and Lemma 3.1.

Lemma 3.4 *(Exterior problem)*
If k^2 is not a Dirichlet eigenvalue of Ω_0, then under the conditions of Lemma 3.2 on Γ_0 a solution $\varphi \in H_{(\frac{1}{2})}(\Gamma)$ to the equation (12) is unique and a solution $(\varphi_0, \varphi_1) \in H_{(\frac{1}{2})} \times H_{(-\frac{1}{2})}(\Gamma)$ to the Helmholtz-Kirchhoff system (18),(19) is unique.

This follows directly from Theorem 3.2, Lemma 2.2 and Lemma 3.2.

4 Approximation and completeness results

Now we discuss approximation of general solutions u by simple solutions. Our goal is to interpolate our data on Γ_0 for further solution of integral equations. This can be crucial for larger k. More importantly, we justify the very efficient HELS method of Sean Wu, see [IW], [Wu].

Theorem 4.1 *Let Ω be a bounded Lipschitz domain in $\mathbf{R}^\mathbf{n}$, and let $u \in H_{(1)}(B \setminus \overline{\Omega})$ be a radiating solution to the Helmholtz equation $\Delta u + k^2 u = 0$ in Ω_+. For any $a \in \Omega$ and any positive ε, there is a radiating solution u_ε to the Helmholtz equation outside a such that*

$$\|u - u_\varepsilon\|_{(1)}(\Omega_+ \cap B) < \varepsilon. \tag{20}$$

We outline a proof. By extension theorems for Sobolev spaces in Lipschitz domains, see [I], there is an extension $u^* \in H_{(1)}(B)$ of u onto $\mathbf{R^n}$. Let $f^* = \Delta u^* + k^2 u^*$. Clearly, $f^* \in H_{(-1)}(\mathbf{R^n})$ and *supp* $f^* \subset \overline{\Omega}$. It is known that $f^* = f_0 + \sum \partial_j f_j$ for some functions $f_0, ..., f_n \in L_2(\mathbf{R^n})$ supported in $\overline{\Omega}$. Let χ_m be a sequence of measurable functions with values 0 or 1 supported in Ω and convergent to 1 a.e. on Ω. Then the sequence $f^*_m := f_0\chi_m + \sum \partial_j (f_j \chi_m)$ converges to f in $H_{(-1)}(\mathbf{R^n})$ and *supp*$f^*_m \subset \Omega$. It is well-known in the theory of elliptic equations, (see [I], section 4.1), that radiating solutions to the Helmholtz equition $(\Delta + k^2)u_m = f^*_m$ in $\mathbf{R^n}$ converge to u in $H_{(1)}(B \setminus \overline{\Omega})$. Therefore, one can find u_m such that

$$\|u - u_m\|_{(1)}(B \setminus \overline{\Omega}) < \frac{\varepsilon}{2}.$$

Due to uniqueness of the continuation and the Runge property for the Helmholtz equation, there is a radiating solution u_ε to the Helmholtz equation outside a such that

$$\|u_m - u_\varepsilon\|_{(1)}(B \setminus \overline{\Omega}) < \frac{\varepsilon}{2}.$$

From the last two inequalities we obtain (20) and the proof is complete.

In some applications in $\mathbf{R^3}$, it is very helpful to use the special family of radiating solutions to the Helmholtz equation given by

$$e_{n,m}(x) = h_n^{(1)}(kr) Y_{n,m}(\sigma), \tag{21}$$

where $h_n^{(1)}$ is the spherical Hankel function of the first kind and $Y_{n,m}$ are spherical harmonics orthonormal in $L_2(S^2)$ on the unit sphere S^2. We set out to approximate solutions u to the Helmholtz equation by linear combinations of the form

$$u_e(x) = \sum u_{n,m} e_{n,m}(x), \qquad m = 0, ..., 2n+1, \qquad n = 0, ..., N. \tag{22}$$

The following lemma demonstrates that such approximation is indeed possible.

Lemma 4.1 *Let* $0 \in \Omega$ *and* $u \in H_{(1)}(B \setminus \overline{\Omega})$ *be a radiating solution to the Helmholtz equation. For any positive* ε *there is* u_e *of the form* (21) *such that*

$$\|u - u_e\|_{(1)}(B \setminus \overline{\Omega}) < \varepsilon. \tag{23}$$

By Theorem 4.1 there is a radiating solution u_ε to the Helmholtz equation in $\mathbf{R}^3 \setminus \{0\}$ such that $\|u - u_\varepsilon\|_{(1)}(B \setminus \overline{\Omega}) < \frac{\varepsilon}{2}$. Let B_1 be a ball of radius r_1 centered at 0 such that $\overline{B_1} \subset \Omega$. The spherical harmonics $Y_{n,m}$ form an orthonormal basis in $L_2(S^2)$. Expanding the function $u_\varepsilon(r_1\sigma)$ with respect to this basis we conclude, that the partial sums of the corresponding series are convergent in $L_2(\partial B_1)$, and hence (see e.g. [CoKr], Theorem 2.14) they converge to u_ε in $L_2(B \setminus \bar{B}_1)$. One can thus find a partial sum u_e such that $\|u_\varepsilon - u_e\|_{(1)}(B \setminus \bar{\Omega}) < \frac{\varepsilon}{2}$. Now the claim follows from the triangle inequality.

A similar result is valid for interior problems, if one replaces the functions $e_{n,m}$ by the functions $E_{n,m}(x) = j_n(kr)Y_{n,m}(\sigma)$.

We now discuss how to use these results to approximate u by u_e. Let Ω_* be a subdomain of $B \setminus \Omega$. Setting $\varepsilon = 1$ in (23), we conclude that for $\varepsilon < 1$ there exist approximating functions u_e such that

$$\|u_e\|_{(1)}(\Omega_*) \leq M_1 = \|u\|_{(1)}(B \setminus \bar{\Omega}) + 1. \tag{24}$$

A weaker version of this constraint is

$$\|u_e\|_{(0)}(\Omega_*) < M_0 \leq M_1. \tag{25}$$

Since the data are given on Γ_0, one can try to approximate u by u_e by solving the minimization problem

$$\min \|u - u_e\|_{(0)}(\Gamma_0)$$

subject to the constraint (24) or the weaker constraint (25). Solving this problem for a sufficiently large $N = N(\delta)$, one finds $u_e(;\delta)$ such that

$$\|u - u_e(;\delta)\|_{(0)}(\Gamma_0) < \delta, \tag{26}$$

and that the constraint (25) holds.

In the following lemma, we denote by $\Omega_{*,d}$ the collection of points of Ω_* which are at distance d from $\partial\Omega_* \setminus \Gamma_*$.

Lemma 4.2 *Let Ω_0 be a bounded domain and either i) $\bar{\Omega} \subset \Omega_0$ or ii) $\bar{\Omega}_0 \subset \Omega_+$. If k^2 is distinct from a Dirichlet eigenvalue of Ω_0, then there are positive constants C and $\lambda < 1$ depending on Γ, Ω_*, d and k, such that*

$$\|u - u_e\|_{(0)}(\Omega_{*,d}) \leq C\left(\delta + M^{1-\lambda}\delta^{\lambda}\right).$$

In addition, if $\Omega_* \subset conv(\Gamma_0)$, the convex hull of Γ_0, then there are constants C and $\lambda < 1$ depending on Γ, Ω_* and d, such that

$$\|u - u_e\|_{(1)}(\Omega_{*,d}) \leq C\left(\delta + \frac{M^{1-\lambda}\delta^{\lambda}}{1+k}\right).$$

In case i), we can uniquely solve the exterior Dirichlet problem for $u - u_e$ outside Ω_0, and in case ii) the interior Dirichlet problem. In both cases, $C\delta$ bounds the Cauchy data for $u - u_e$ on some surface Γ_1 which is close to Γ_0. Thus Lemma 4.2 follows from (3) and Theorem 2.2.

The second bound of Lemma 4.2 shows that stability in the convex hull of Γ_0 increases with k. We note that in our stability and convergence results, the parameter d is the distance to the boundary of the domain, where u satisfies the Helmholtz equation. Intuitively, d is the closest distance from $\Omega_{*,d}$ to singularities of u. Hölder stability and convergence are obtained in interior subdomains $\Omega_{*,d}$. By introducing the domain Ω_*, we emphasize the local character of the problem. If one is interested in some part Ω_* of Ω_+, employing the constraint (25) gives rise to approximations u_e convergent only in Ω_*.

5 Numerical methods

In this section we describe our numerical methods for the single layer representation, the Helmholtz-Kirchhoff system, and the Helmholtz Equation Least Squares (HELS) of Sean Wu. In Section 6, we discuss regularization for the resulting linear problems, and in Section 7, we give some sample numerical results comparing these methods in some representative problems in two and three dimensions. The numerics for the 2D case uses a Nyström method presented in [CoKr], Section 3.5, who follow an approach by Kussmaul [K]. For the 3D case [DIVW2], [DHV], we have developed a boundary element code based the FORTRAN code in [AT1], [DIVW2] using piecewise linear triangular elements. All the programing has been done in MATLAB and run on PCs.

5.1 The Single Layer approach

In this case, the solution $u(x)$ is represented in Ω by the single layer potential. One solves the integral equation (12). In [DIVW1], [DIVW2], [DHV], this approach has been shown to be straightforward and efficient. $N-$point discretizations of equations (12), (13) give rise to the $N \times N$ systems

$$S_{0,N}\varphi_N = U_N,$$

and

$$v_N = \frac{1}{2}\varphi_N + K_N\varphi_N$$

for the single layer method for the interior problem.

5.2 The Helmholtz-Kirchhoff Approach

Our second approach uses the systems of the integral equation (16), (17) for the interior problem. The equations above may be written instructively in a block form as

$$H\begin{pmatrix} u_\Gamma \\ v_\Gamma \end{pmatrix} := \begin{pmatrix} \frac{1}{2}I + D_\Gamma & -S_\Gamma \\ -D_{\Gamma_0} & S_{\Gamma_0} \end{pmatrix}\begin{pmatrix} u_\Gamma \\ v_\Gamma \end{pmatrix} = \begin{pmatrix} 0 \\ U \end{pmatrix}.$$

An N-point discretization of these equations gives rise to the $2N \times 2N$ system

$$H_N\begin{pmatrix} u_N \\ v_N \end{pmatrix} := \begin{pmatrix} \frac{1}{2}I_N + D_N & -S_N \\ -D_{0,N} & S_{0,N} \end{pmatrix}\begin{pmatrix} u_N \\ v_N \end{pmatrix} = \begin{pmatrix} 0_N \\ U_N \end{pmatrix}$$

for the Helmholtz-Kirchhoff approach for U given on Γ_0.
Remark: A standard method in the acoustics literature is to solve the system for v_Γ involving the Neumann Green's function

$$Gv_\Gamma := (S_{\Gamma_0} - D_{\Gamma_0}(\frac{1}{2}I + D_\Gamma)^{-1})v_\Gamma = U.$$

This setup requires the inversion of the (generally well-posed) operator $\left(\frac{1}{2}I + D_\Gamma\right)$. When Ω has a separable geometry, an explicit formula can be obtained for G leading to very efficient numerical methods; see [Wil1] for further discussion. However, for general geometries, the computation of G is expensive compared with the present methods; see [DHV], [VW].

5.3 The HELS method

The Helmholtz Equation Least Squares (HELS) method, proposed by Sean Wu, aims to reconstruct time-harmonic acoustic pressure represented in terms of spherical wave functions. A theoretical justification is presented in [IW] and [Wu]. In the presence of noise, it is natural to view HELS as a regularization method with the number of the expansion terms regarded as a regularization parameter.

In two dimensions, the radiating accoustic pressure is approximated by basis functions of the form

$$\begin{aligned} e_n(re^{it}) &= H_n^{(1)}(kr)\, e^{int}, \\ e_{-n}(re^{it}) &= H_n^{(1)}(kr)\, e^{-int}, \end{aligned}$$

where $H_n^{(1)}$ is the Hankel function of the first kind for $n = 0, 1, 2, \ldots$.

The expansion coefficients are found by fitting pressure measurements data at the points $x_1, \ldots, x_n$ with linear combinations of these basis functions

$$u(x_k) \approx \sum_{m=-N}^{N} a_m e_m(x_k),$$

$k = 1, \ldots, n$. Once the coefficients a_m ($|m| \leq N$) are found, the normal velocity can be approximated using Euler's equation, by formally differentiating the expansion for pressure:

$$v(x) \approx \frac{1}{ik\rho_0 c} \sum_{m=-N}^{N} a_m \frac{\partial e_m}{\partial \nu}(x),$$

where ρ_0 is the ambient density of the fluid medium, and c is the speed of sound in the medium. In the special case of radial geometry, the outward normal derivative $\frac{\partial}{\partial \nu}$ coincides with the radial derivative, and, consequently,

$$\begin{aligned} \frac{\partial e_0}{\partial \nu}(re^{it}) &= -kH_1^{(1)}(kr), \\ \frac{\partial e_n}{\partial \nu}(re^{it}) &= \frac{k}{2}\left[H_{n-1}^{(1)}(kr) - H_{n+1}^{(1)}(kr)\right] e^{int}, \\ \frac{\partial e_{-n}}{\partial \nu}(re^{it}) &= \frac{k}{2}\left[H_{n-1}^{(1)}(kr) - H_{n+1}^{(1)}(kr)\right] e^{-int}, \end{aligned}$$

for $n = 1, 2, \ldots$.

6 Regularization

We solve linear systems

$$Ax = b, \tag{27}$$

where A is a complex $n \times n$ matrix and x and b are $n-$ vectors with $n = N$ for $S_{0,N}$ and $n = 2N$ for H_N. In a real situation the data b contain measurement errors e and we denote

$$b^\delta = b + e,$$

where e is a random vector with $\|e\|_2 = \delta \|b\|_2$ and δ is the percentage of error. The linear systems (27) are ill-posed. Therefore the errors e are amplified in the solution x, and the recovered x is useless. Hence regularization methods are required to filter the effects of the errors.

The analysis and implementation of our regularization methods are based on the Singular Value Decomposition (SVD). The SVD of A is the decomposition

$$A = U\Sigma V^* = \sum_{i=1}^{n} \sigma_i u_i v_i^* \tag{28}$$

where $U = (u_1, ..., u_n) \in \mathbb{C}^{n\times n}$ and $V = (v_1, ..., v_n) \in \mathbb{C}^{n\times n}$ are matrices with orthonormal columns, $U^*U = V^*V = I_n$, and where $\Sigma = diag\,(\sigma_1, ..., \sigma_n)$ with $\sigma_1 \geq \sigma_2 \geq \cdots \geq \sigma_n \geq 0$. The ill-conditioning of A is determined by its condition number σ_1/σ_n and the rate of decrease of the singular values, σ_i.

In the next subsections we describe the regularization methods used in the numerical experiments of this paper.

6.1 Truncated Singular Value Decomposition.

The solution to least squares problem

$$\min_x \|Ax - b^\delta\|_2$$

is given by

$$x_{LS}^\delta = \sum_{i=1}^{n} \frac{u_i^* b^\delta}{\sigma_i} v_i = \sum_{i=1}^{n} \frac{u_i^* b}{\sigma_i} v_i + \sum_{i=1}^{n} \frac{u_i^* e}{\sigma_i} v_i. \tag{29}$$

where in the case of ill-posed linear systems $|u_i^* b|$ decreases with the same rate as σ_i. The first term in last expression in (29) corresponds to the noiseless solution, while the second term contains the error term. The error term has the property that $|u_i^* e|$ tends to a constant $|u_i^* e| \approx |u_i^* b^\delta| \approx \delta$ with increasing i. The decay of the singular values of A then causes $\left|u_i^* b^\delta\right| / \sigma_i$ to increase significantly, affecting the solution. A regularization method is used to reduce the effect of the noise term in the solution.

The truncated SVD (TSVD) method truncates the solution after the first m terms, giving the regularized solution

$$x_m = \sum_{i=1}^{m} \frac{u_i^* b^\delta}{\sigma_i}\, v_i. \tag{30}$$

The number m of retained terms is the regularization parameter in this case. A simple stopping strategy is to truncate the expansion at the index corresponding to the coefficient with the smallest magnitude. This observation is the basis of our stopping rule for CGNE discussed next.

6.2 Conjugate gradient for the normal equations via Lanczos bidiagonalization.

Here we summarize the algorithm and heuristic stopping rule given in [DH] and applied in [DHV] in an earlier, slightly different form.

The conjugate gradient algorithm applied to the normal equations (CGNE)

$$A^*Ax = A^*b^\delta$$

at the m-th step minimizes the A^*A–norm error

$$\|x - x_m\|_{A^*A} = \|A(x - x_m)\|_2^2 = \|b^\delta - Ax_m\|_2^2$$

over the m-th Krylov subspace,

$$K_m(A^*A, A^*b^\delta) = \operatorname{span}\left(A^*b, (A^*A)A^*b, \ldots, (A^*A)^{m-1}A^*b\right).$$

We also note that the conjugate gradient method finds the optimal solution in the first several iterations and then diverges rapidly toward the solution to the problem with noisy data. This regularizing behavior is due to the fact that conjugate gradient initially reduces the error in the direction of the dominant (low frequency) singular vectors v_i ($A^*Av_i = \sigma_i^2 v_i$) which are less corrupted by noise relative to the high frequency modes corresponding to small σ_i's. The rapid convergence-divergence behavior, known as semi-convergence, is often more pronounced for the conjugate gradient than the for the TSVD and the choice of the regularization parameter m – the "stopping rule" – is thus crucial.

It is well-known, that the CGNE algorithm can be implemented via the Lanczos bidiagonalization process, see [GvL]. Our approach is to seek regularized solutions within the Krylov subspaces of A^*A. We use the SVD of the bidiagonal matrix B_m generated by the Lanczos process to construct a new basis for $K_m(A^*A, A^*b^\delta)$, which plays the role of the right singular vectors of A. We then compute the expansion coefficients of x_m in this basis and apply the stopping method described below. Specifically, we choose m to minimize the magnitude of the m-th coefficient of x_m. A formal description follows.

Given perturbed data b^δ with $\|b^\delta - b\|_2 = \delta\|b\|_2$, we apply the conjugate gradient algorithm to the normal equations $A^*Ax = A^*b^\delta$. We use the Lanczos bidiagonalization process to construct a lower bidiagonal matrix B_m and two rectangular matrices U_{m+1} and V_m with orthonormal columns such that

$$AV_m = U_{m+1}B_m, \tag{31}$$

and $\frac{b^\delta}{\|b^\delta\|_2}$ is the first column of U_{m+1}. Let

$$B_m = \tilde{U}_m\tilde{\Sigma}_m\tilde{V}_m^*$$

be the singular value decomposition of B_m. The columns $u_1^m, u_2^m, \ldots, u_m^m$ of $U_m\tilde{U}_m$ form an orthonormal basis of the Krylov subspace $K_m(AA^*, b^\delta)$, while the columns $v_1^m, v_2^m, \ldots, v_m^m$ of $V_m\tilde{V}_m$ an orthonormal basis of the Krylov subspace $K_m(A^*A, A^*b^\delta)$. To describe our parameter selection rule, we compute the coefficients of the approximate solution x_m as represented in the basis $v_1^m, v_2^m, \ldots, v_m^m$. It can be shown [DH] that

$$x_m = \|b^\delta\|_2\, V_m\tilde{V}_m\tilde{\Sigma}_m^{-1}\tilde{U}_m(1,:)^* = \|b^\delta\|_2 \sum_{i=1}^{m} \frac{\overline{\tilde{U}_m(1,i)}}{\tilde{\Sigma}_m(i,i)}\, v_i^m.$$

Up to a constant factor, the magnitude of the m-th coefficient is given by the formula

$$\psi_m = \left|\frac{\tilde{U}_m(1,m)}{\tilde{\Sigma}_m(m,m)}\right|.$$

We find the value $m = m_0$ where the sequence $\{\psi_m\}$ has a global minimum and choose x_{m_0} as our approximation to x. This is our stopping rule for choosing the optimal regularization parameter, m_0.

For the reader's convenience, we restate the algorithm from [DH] for computing the quantities x_m and ψ_m. Note the reorthogonalization steps which are needed to avoid computation of "ghost" singular which can interfere with the algorithm.

Algorithm

$U(:,1) = b^\delta/\|b^\delta\|_2$
$V(:,0) = \mathbf{0}$
$B(1,0) = 0$
for $m = 1, 2, \ldots$
    $p = A^* * U(:,m) - B(m,m-1) * V(:,m-1)$
    $p = p - V(:,1:m-1) * (V(:,1:m-1)^* * p)$ (reorthogonalization)
    $B(m,m) = \|p\|_2$
    $V(:,m) = p/B(m,m)$
    $q = A * V(:,m) - B(m,m) * U(:,m)$

$q = q - U(:,1:m) * (U(:,1:m)^* * q)$ (reorthogonalization)
$B(m+1,m) = \|q\|_2$
$U(:,m+1) = q/B(m+1,m)$
$\left[\tilde{U},\tilde{\Sigma},\tilde{V}\right] = \text{svd}(B(1:m+1,1:m))$ (the reduced SVD)
$\psi_m = |\tilde{U}(1,m)/\tilde{\Sigma}(m,m)|$
$x_m = \|b^\delta\|_2 \, V(:,1:m)\tilde{V}\tilde{\Sigma}^{-1}\tilde{U}(1,:)^*$
end

Since the smallest singular value and the corresponding left singular vector of $\tilde{\Sigma}_m$ can be found in $O(m)$ operations, for a large m the cost of the m-th step is dominated by reorthogonalization and is $O(mn)$.

7 Numerical results.

We give three examples of numerical calculations illustrating our theoretical results and comparing the alternative methods. In Example 1, we compare the single layer and Helmholtz-Kirchhoff approach for a two dimensional problem where Ω is the interior of a disk and the exact solution is a point source outside the disk. The Lanczos/CGNE stopping rule is compared with TSVD and the behavior of CGNE is explained in terms of the singular values of the systems. In Example 2, we illustrate the effectiveness of the single layer approach combined with the CGNE stopping rule on a three dimensional problem using actual experimental data taken on Ω the interior of a cylindrical aircraft fuselage section. A similar problem involving a cylinder with a floor was treated in [DHV] with good results. Both examples exhibit geometry with edges. In Example 3, we compare the single layer approach with the HELS method in two dimension for a problem on the exterior of a disk where data are taken and recovered locally on arcs.

We solve the system (27) for a range of wave numbers k. Recall that $k = \omega/c$, where ω denotes the frequency and c is the speed of sound. In the case of the interior aircraft cabin noise $c = 350\ m/\sec$ and the range of interest of ω is typically in the range of human speech

$$20\pi/\sec < \omega = 2\pi f < 1000\pi/\sec,$$

where f is the frequency in Hertz. this leads to a range of k of

$$0.06\pi/m < k < 3\pi/m.$$

Since the cabin dimensions a are on the order of meters, the dimensionless quantity ka has a similar range.

Example 1. In this case Γ is the unit circle in two dimensions and Γ_0 is the circle of radius 0.9 centered at the origin. The exact test case is a point source $u(x) = \Phi(x, x_0)$, with the point $x_0 = (.5, 1.5)$ exterior to Ω. The normal velocity v on Γ can then be computed exactly. We report relative errors in v, in the 2-norm for each iteration m, $||v - v_m||_2/||v||_2$. The noise level is $\delta = .01$.

The results of numerical experiments for typical values of the wavenumber k are given Figures 1 and 2. Figure 1 shows the influence of the singular values of the matrices $S = S_{0,N}$ and $H = H_N$ on the relative errors in the velocity on Γ computed with Lanczos/CGNE for S and H and TSVD for S. Note that the about half of the singular values of the Helmholtz-Kirchhoff H system are grouped around 1/2, since the (1,1) block $(1/2)I_N + D_N$ of H is (1/2) times the identity plus a compact operator. The other blocks are discretizations of compact operators and cause the leading and trailing first N singular values to be perturbed above and below 1/2 and the last N singular values to decay rapidly to 0. The leading singular values of S have roughly the same distibution as the last N singular values of H, since the (2,2) block of H is just S. This distribution of the singular values is this reason H requires more than twice as many conjugate gradient iterations as the single layer system to find the optimal regularized solution. The singular values grouped near 1/2 only cause about one additional CGNE iteration. However, many more terms (about N) would be required in the TSVD for H (not shown here) to represent the optimal regularized solution. The number of terms required in the TSVD of S for the regularized solution is about twice the number of CGNE iterations due to the fact that the multiplicity is two for most of the singular values of S for the disk. The grouping of the singular values is smeared slowly with increasing k, causing a small, but noticeable, increase in the number of CGNE iterations in the two dimensional case. This effect is much more noticeable in three dimensions where for typical geometries, e.g., the sphere in Example 3, the multiplicity of the singular values σ_i of S increases with i.

Figure 2 compares how well our stopping rule - choose the solution x_i such that ψ_i is a (local) minimum - predicts the optimal regularized solution for S and H for this example. As reported in [DH], [DHV], the stopping rule is usually within one iteration of the optimal solution. Note that with $N = 80$, there is a loss of resolution as k increases and the stopping rule becomes less reliable, especially for H.

Example 2. This example uses data taken on a cylindrical test section (Γ) from a Cessna business jet at the U. S. Naval Research Laboratory. A 64×32 array of microphone measurements is taken on a concentric cylindrical surface (Γ_0) in the nearfield. The (exact) velocity on Γ was also measured. The pressure data is Fourier analyzed into over 1000 frequencies. We only analyze two frequencies, $98.9MHz$ in Figure 3 and $164.8MHz$ in Figure 4 corresponding to $k \approx 1.8/m$ and $k \approx 3.0/m$, respectively. We use S, alone, to demonstrate the effectiveness of the combination of our new stopping rule with the single layer representation to reconstruct the velocity on the fuselage.

The upper left hand frame in Figures 3 and 4 displays the exact velocity. The x-axis of the plot is parallel to the center axis of the cylinder and the y-axis is parallel

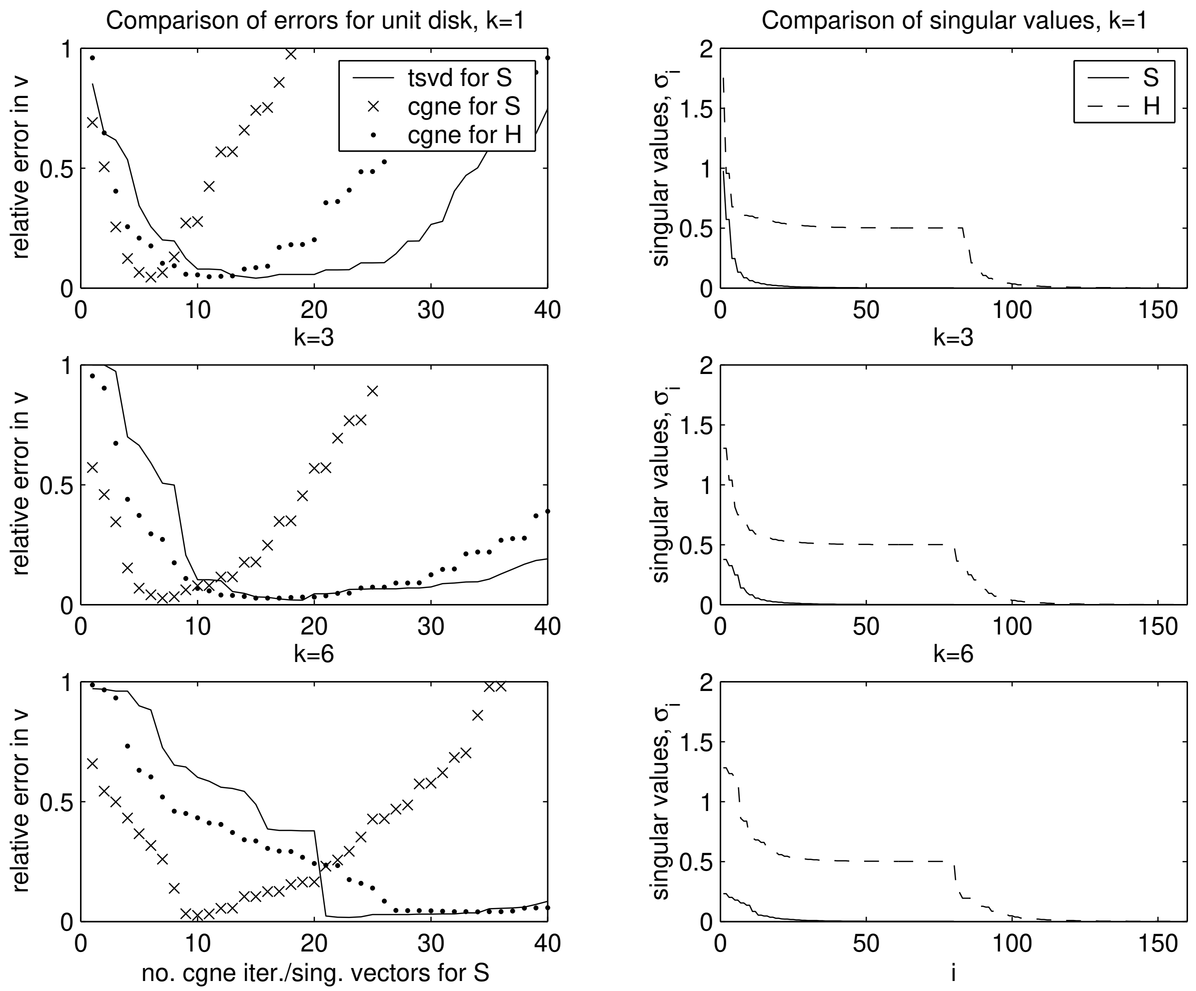

Figure 3: Comparison of relative errors in velocity and singular values for Example 1, the unit disk, with $S = S_{0,N}, H = H_N, N = 80, \delta = .01$, and a point source located at $(.5, 1.5)$

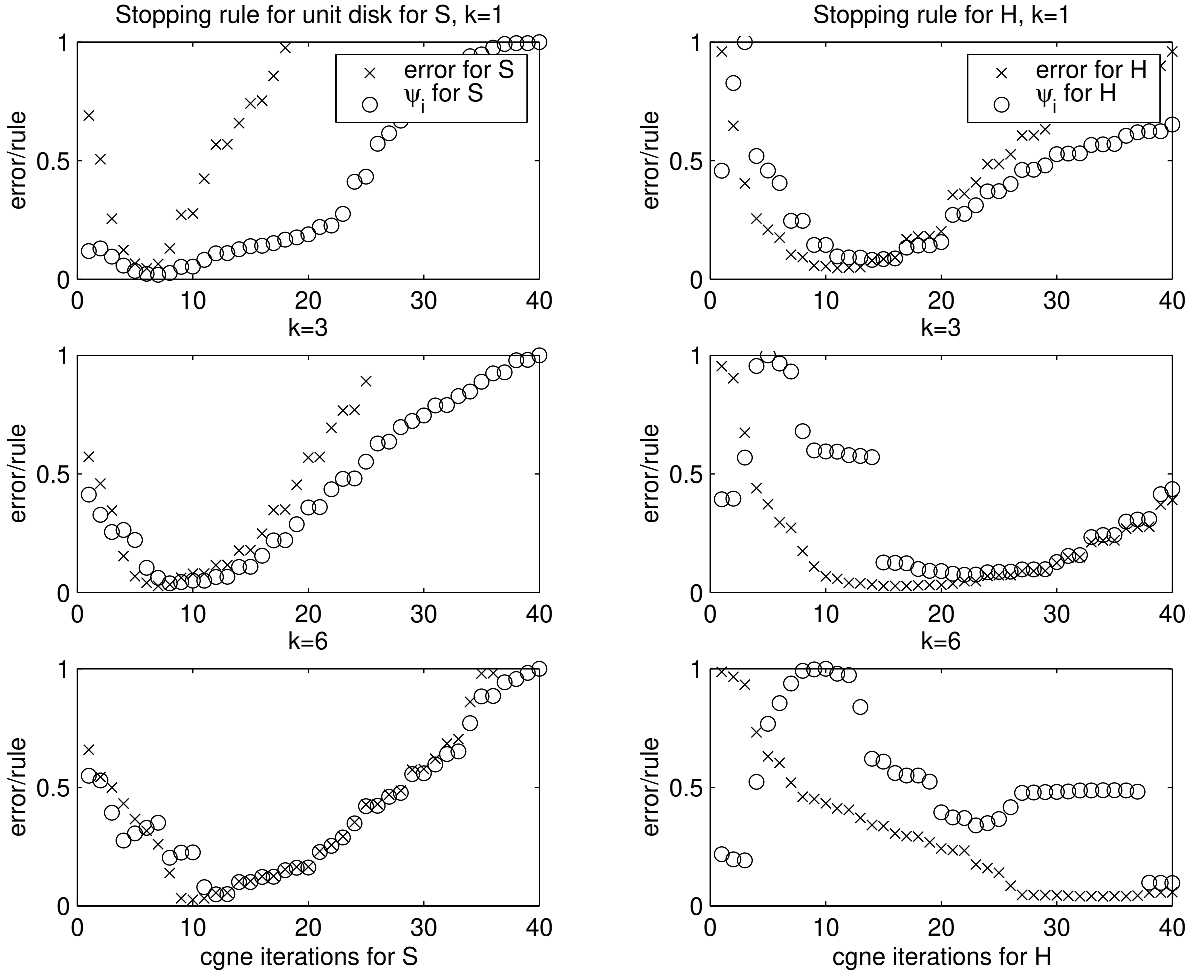

Figure 4: Comparison of the stopping rule for Example 1, the unit disk, with $S = S_{0,N}, H = H_N, N = 80, \delta = .01$, and a point source located at $(.5, 1.5)$

to the circumference. The upper right hand plot is the stopping rule ψ_i (solid line) with the minimum circled. Often a local minimum gives a good choice for the optimal solution. The dashed line is the norm of the difference between successive iterates i of the density $||\varphi_{i+1} - \varphi_i||$. When these successive variations have settled down, it provides an indication that the optimal regularized solution has been reached. (Montoring these variations was suggested by G. Majda (personal comunication). It is useful, in practice, to have more than one method to choose the regularization parameter.) The remaining four frames in the Figures display the reconstructed velocity at the indicated CGNE iterates. The optimal solution is displayed. Note that it captures many of the features of the exact velocity. The early iterates are overregularized (oversmoothed) and the latter iterates become underregularized (undersmoothed) and exhibit the effects of amplified measurement errors. The matrices S and K are 1282×1282 and it takes about 2 seconds per CGNE iteration to produce the velocity plots. One can therefore easily watch the successive iterates "tune"to the optimal solution. The BEM construction of the matrices S and K, and the SVD of the full matrix S for the TSVD take about 20 minutes each on a 950 MHz PC.

We note that only about every second NRL circumferential data point was used in our computations (hence, the different scales on the y-axes of the displays), so that our higher frequency calculation may be somewhat underresolved. In addition, the endcap data may have been slightly missaligned. Nevertheless, the reconstructions are quite reasonable. The bright "hotspots" are at the window locations. We plan more extensive tests on laboratory data in the future.

Example 3. In this example we describe our numerical experiments devoted to the reconstruction of the normal velocity along a curve from the acoustical pressure. We consider three concentric arcs Γ, Γ_{01} and Γ_{02} defined as follows:

$$\Gamma = \{x : \|x\| = r_0, \theta_1 < \arg(x) < \theta_2\}, \tag{32}$$

$$\Gamma_{01} = \{x : \|x\| = r_1, \phi_1 < \arg(x) < \phi_2\}, \tag{33}$$

$$\Gamma_{02} = \{x : \|x\| = r_2, \phi_1 < \arg(x) < \phi_2\}. \tag{34}$$

Figure 1 shows the arcs for some choices of the parameters $\theta_1, \theta_2,\ \phi_1, \phi_2$ used in the experiments, as described in below.

We attempt to recover the outward normal velocity $v = \partial_\nu u$ on arc Γ from the acoustic pressure measurements u on arcs Γ_{01} and Γ_{02}. We employ two methods: one based on a single layer representation of the potential, and the HELS method proposed by Sean Wu, see [Wu].

The charge density φ is computed from the pressures $u(x)$ on arcs Γ_{01} and Γ_{02}, and then the normal velocity on arc Γ is found from the formula (13). The operator K used above is defined as the second term in (13).

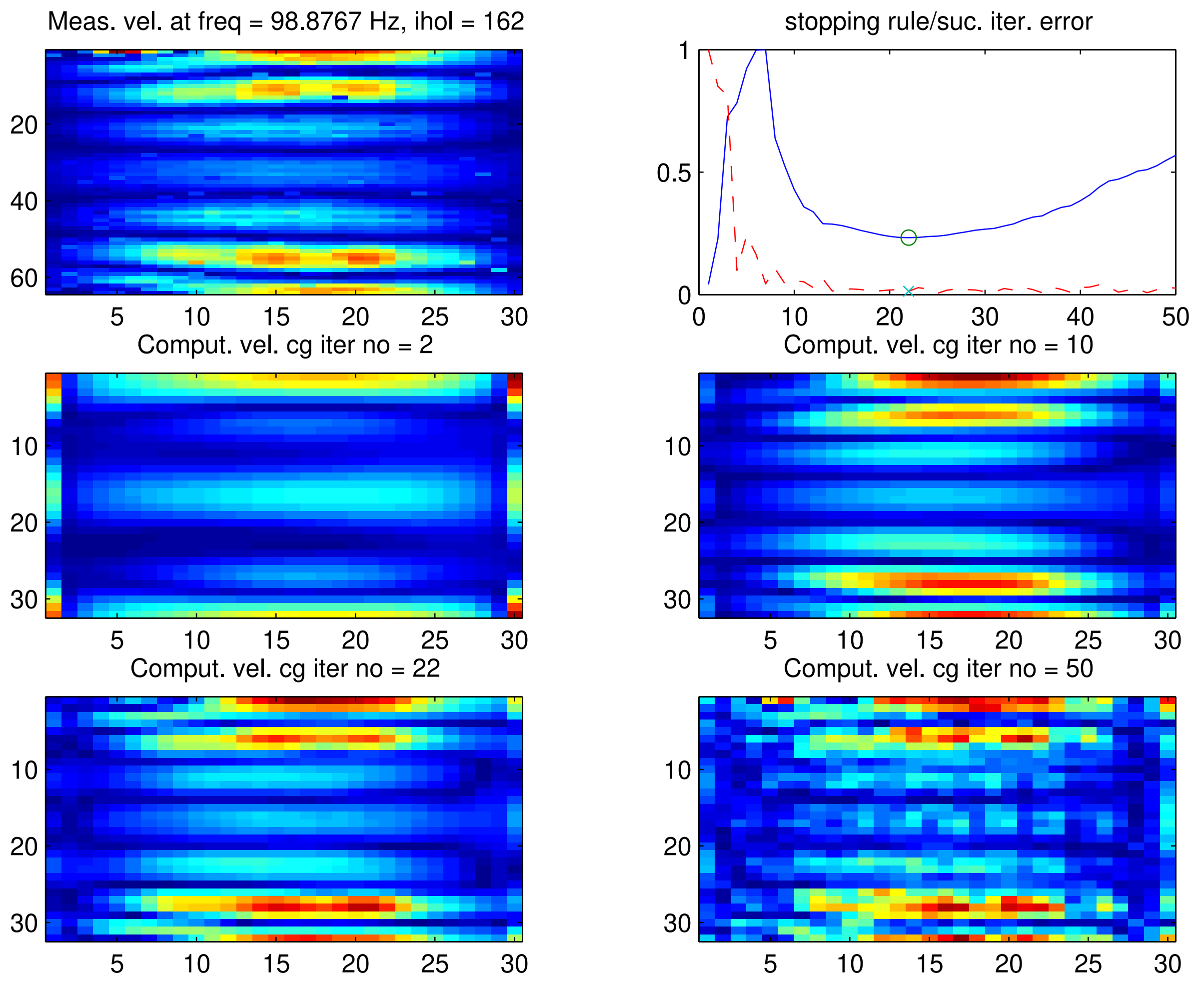

Figure 5: Lanczos/CGNE on NRL/Cessna test section data using S with frequency 98.9 Hz, N = 1282

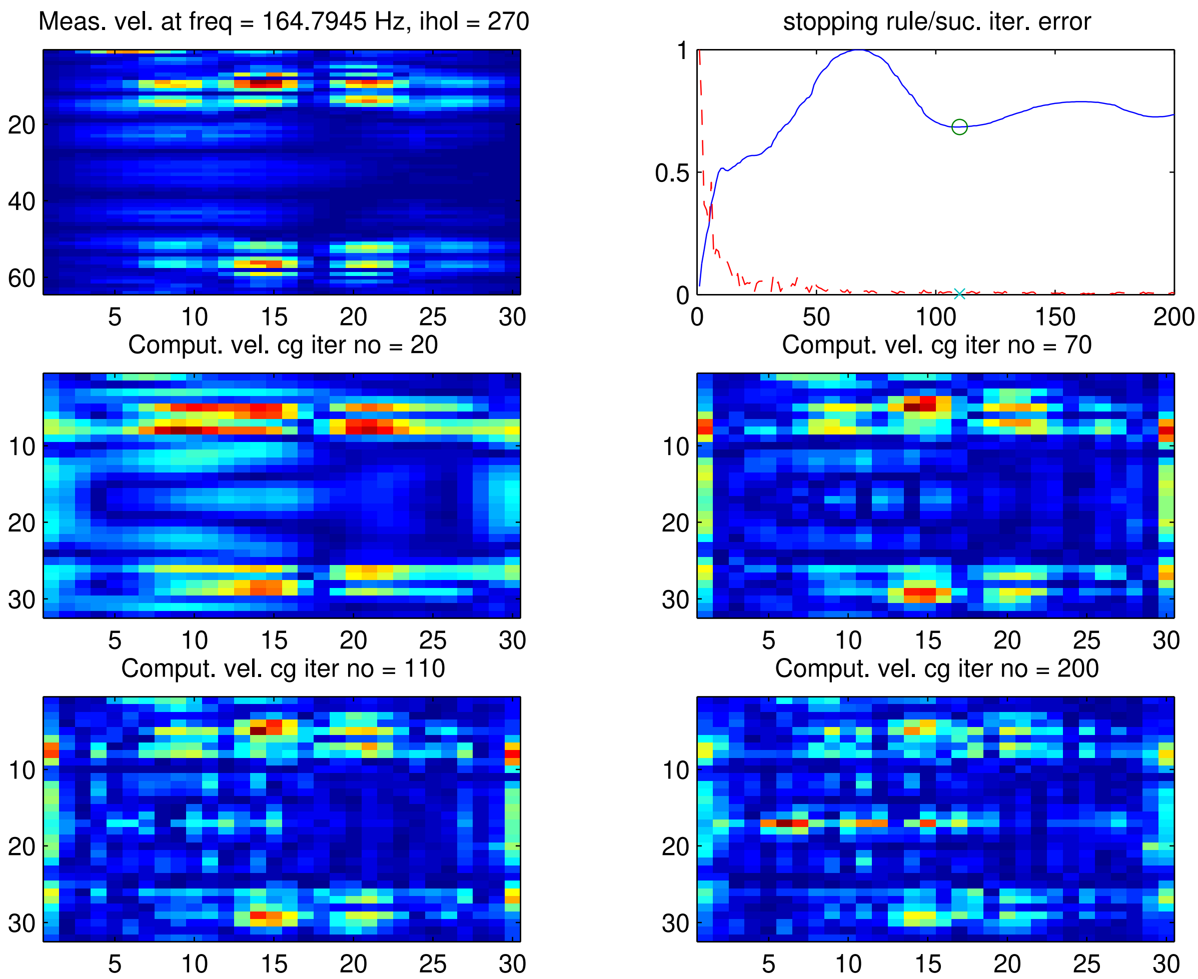

Figure 6: Lanczos/CGNE on NRL/Cessna test section data using S with frequency 164.8 Hz, N = 1282

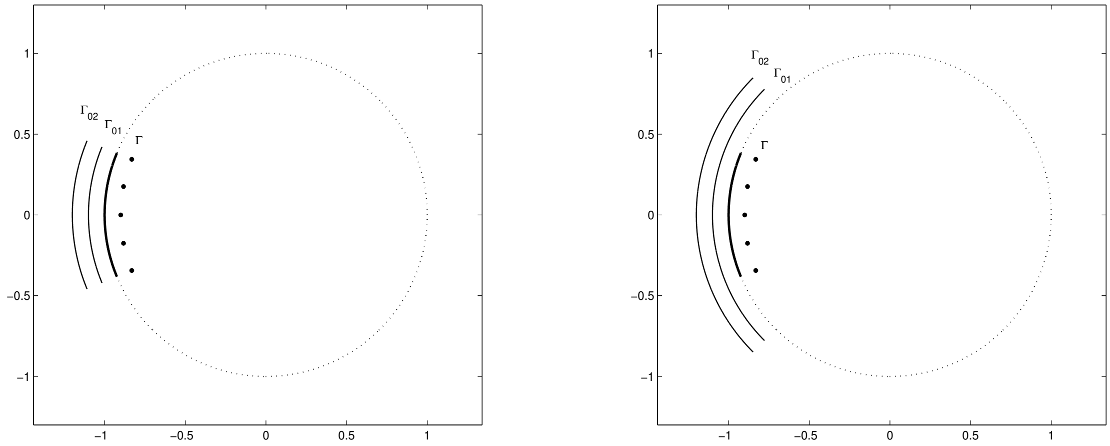

Figure 7: The arcs Γ, Γ_{01}, and Γ_{02} in two experiments.

We perturb the exact pressures u by adding noise of the relative intensity $\delta > 0$. Our simulated measurements are thus $u^\delta = u + \xi$, where ξ is a random vector with $\|\xi\|_2 = \delta\|u\|_2$. The system $S_n\varphi = u^\delta$ is solved using the Conjugate Gradient on the Normal Equations (CGNE). For each $m = 1, 2, \ldots$, we obtain a regularized charge density φ_m. Then we create a sequence of approximate normal velocities $v_N = K_N\varphi_N$. We choose the iteration number m_0 to minimize the relative L_2 error of the normal velocities

$$\mathrm{err}_m = \frac{\|v - v_m\|_2}{\|v\|_2}. \tag{35}$$

We denote the minimal error by err_0:

$$\mathrm{err}_0 = \min_m \ \mathrm{err}_m. \tag{36}$$

We describe of this approach in Experiment 1.

Experiment 1. We first consider arcs Γ_{01} and Γ_{02}, respectively, described by equations (33), (34) with parameters $\phi_1 = \frac{7\pi}{8}$, $\phi_2 = \frac{9\pi}{8}$, $r_1 = 1.05$, and $r_2 = 1.10$. Arc Γ is given by (32) with parameters $r = 1$, $\theta_1 = \frac{7\pi}{8}$, $\theta_1 = \frac{9\pi}{8}$, as in Figure 1 on the left. We place acoustic charges with strengths $w_1, w_2, ..., w_p$ at the points $x_1, x_2, ..., x_p$, and thus the resulting pressure u is given by

$$u(x) = \sum_{i=1}^{p} w_i \, \Phi(x, x_i). \tag{37}$$

We use $p = 5$ charges with strengths and locations given in Table 1. The pressures are perturbed with noise of the relative intensity $\delta = 0.01$.

Table 2 presents the minimal relative errors of the normal velocities v_m as defined in (36) for wave numbers $k = 1, 3, 6, 12$. The second column of the table contains err_0^1,

1.0	(-0.73910, 0.30615)
4.0	(-0.78463, 0.15607)
5.0	(-0.80000, 0.00000)
2.0	(-0.78463, -0.15607)
3.0	(-0.73910, -0.30615)

Table 1: The strengths and locations of the acoustic charges.

k	err_0^1	err_0^2
1.0	0.084	0.026
3.0	0.065	0.011
6.0	0.036	0.011
12.0	0.029	0.004

Table 2: Relative errors of the normal velocities for the single layer method.

the minimal error corresponding to the wave numbers in the first column when $\phi_1 = \frac{7\pi}{8}$, $\phi_2 = \frac{9\pi}{8}$. The last column contains the relative error err_0^2 when $\phi_1 = \frac{3\pi}{4}$, $\phi_2 = \frac{5\pi}{4}$. Each relative error err_0^1 and err_0^2 is the average over 20 trials.

Experiment 2. We solve the same problems using the HELS method. We approximate the potential with $n = 15$ radial wave functions centered at the origin. The normal velocities are approximated by formally differentiating the basis functions. The relative errors are presented in Table 3. As before, the errors are averged over 20 trials.

We observe immediately that for the layer method, the reconstruction of the normal velocities improves as the wave number k increases. When the HELS method is used, the relative errors are very close to the noise level for all wave numbers considered, so increased stability is visible to a limited extent. In both cases $\mathrm{err}_0^1 > \mathrm{err}_0^2$, which only shows that a better reconstruction is possible with more measurement data.

Acknowledgements. We thank Earl Williams, Brian Houston, and Pete Hedric of the

k	err_0^1	err_0^2
1.0	0.024	0.017
3.0	0.011	0.014
6.0	0.010	0.005
12.0	0.025	0.008

Table 3: Relative errors of the normal velocities for the HELS method.

NRL Physical Acosutics Group for use of the data taken on the Cessna test section in Example 2 and Lianju Wang for help with the MATLAB code for processing the data.

References

[AT1] K. E. Atkinson, *The Numerical Solution of Integral Equations of Seconds Kind*, Cambridge University Press, 1997.

[CoKr] D. Colton and R. Kress, *Inverse Acoustics and Electromagnetic Scattering Theory*, Applied Mathematical Science, **93**, Springer-Verlag, New York, 1992.

[DH] T. DeLillo and T. Hrycak, *A stopping rule for the conjugate gradient regularization method for inverse problems in acoustics,* submitted for publication.

[DIVW1] T. DeLillo, V. Isakov, N. Valdivia, and L. Wang, *The detection of the source of acoustical noise in two dimensions*, SIAM Journal of Applied Math. , **61** (2001), 2104-2121.

[DIVW2] T. DeLillo, V. Isakov, N. Valdivia, L. Wang, *The detection of surface vibrations from interior acoustical pressure*, Inverse Problems, **19** (2003), 507–524.

[DIVW3] T. DeLillo, V. Isakov, N. Valdivia, L. Wang, *Computational methods for the detection of the source of acoustical noise,* Proceedings of the ASME Noise Control Acoustics Division-2000, NCA-Vol. 27, 359–366.

[DHV] T. K. DeLillo, T. Hrycak, N. Valdivia, *Iterative regularization methods for inverse problems in acoustics*, Proc. 2002 ASME Int. Mech. Eng. Congress, New Orleans, LA, IMECE2002/NCA-3270.

[EHN] H. W. Engl, M. Hanke, A. Neubauer, *Regularization of Inverse Problems*, Kluwer, Dordrecht, 1996.

[GvL] G. H. Golub, C. Van Loan, *Matrix Computations*, third edition. Johns Hopkins Studies in the Mathematical Sciences. Johns Hopkins University Press, Baltimore, MD, 1996.

[HI] T. Hrycak, V. Isakov, *Increased stability in the continuation of solutions to the Helmholtz equation*, Inverse Problems **20** (2004), no. 3, 697–712.

[I] V. Isakov, *Inverse Problems for Partial Differential Equations*, Springer-Verlag, New York, 1998.

[IW] V. Isakov, S. Wu, *On theory and application of the Helmholtz equation least squares method in inverse acoustics*, Inverse Problems, **18** (2002), 1147-1159.

[J] F. John, *Continuous dependence on data for solutions of partial differential equations with a prescribed bound*, Comm. Pure Appl. Math., **13** (1960), 551-585.

[K] R. Kussmaul, *Ein numerisches Verfahren zur Lösung des Neumannschen Neumannschen Aussenraumproblems für die Helmholtzsche Schwingungsgleichung*, Computing (Arch. Elektron. Rechnen), **4** (1969), 246–273.

[VW] N. Valdivia and E. G. Williams, *Implicit methods of solution to integral formualtions in boundary element method based nearfield acoustic holography,* submitted for publication.

[Wil1] E. G. Williams, *Fourier Acoustics*, Academic, New York, 1999.

[Wil3] E. G. Williams, *Regularization methods for near-field acoustical holography*, J. Acoust. Soc. Am., **110** (2001), 1976–1988.

[Wu] S. Wu, *Nearfield acoustic holography and its evolution,* submitted for publication.